

Dynamic recrystallization rules in needle piercing extrusion for AISI304 stainless steel pipe

GUO Liang-gang¹, DONG Ke-ke¹, ZHANG Bao-jun¹, YANG He¹, ZHENG Wen-da², LIU Xiong-wei³

1. State Key Laboratory of Solidification Processing, Northwestern Polytechnical University, Xi'an 710072, China;
2. China National Heavy Machinery Research Institute Co. Ltd, Xi'an 710032, China;
3. Sustainable Engineering, University of Cumbria, Energen Campus, Workington CA14 4JW, UK

Received 28 August 2012; accepted 25 October 2012

Abstract: The dynamic recrystallization (DRX) rules are the significant foundation for the effective control of DRX behavior, consequently achieving fine grains and qualified microstructure in the needle piercing extrusion for AISI304 stainless steel pipe. A reliable multi-scale FE model was developed for the extrusion process of seamless AISI304 stainless steel pipe (d_{29} mm \times 4.5 mm) under the DEFORM-2D software environment, and then the influence rules of the key extrusion parameters were numerically unfolded, namely the initial billet temperature and extrusion speed, on the DRX volume fraction, average grain size and their distributions by comprehensive simulations. The outcome establishes the basis and guidelines for the optimal design and steady control of the extrusion process in terms of the microstructure of the extruded pipe.

Key words: AISI304 stainless steel; dynamic recrystallization; needle piercing extrusion; modeling and simulations; microstructure; grain refinement

1 Introduction

The seamless AISI304 stainless steel pipe has been an important profile widely used in oil, transportation and national defense industries mainly due to its excellent corrosion and oxidation resistances and good performance under high and low temperatures [1–3]. With the rapid development of national defense industry and economy, the demand of the seamless AISI304 stainless steel pipes with high strength, high accuracy and excellent corrosion resistance is becoming more and more urgent and extensive [4]. The needle piercing extrusion process, as shown in Fig. 1, has been an irreplaceable forming technology for the manufacture of the seamless AISI304 stainless steel pipe with high performance due to its advantage of improving the formability, the microstructure, dimensional accuracy and surface quality of the extruded pipe [5].

Because the AISI304 stainless steel is a single-phase austenite alloy, it is difficult to refine grains of the alloy by heat treatment. But due to the low stacking fault energy of this alloy, its grain can be

effectively refined by dynamic recrystallization (DRX) under high temperature plastic deformation. So exploring the DRX rules under the key extrusion parameters, such as the initial billet temperature and extrusion speed, has been a significant issue for the optimal design and steady control of the extrusion process in terms of the microstructure of the extruded tube.

Up till now, many studies on the dynamic recrystallization behavior of AISI304 stainless steel in plastic deformation process were carried out by many researchers [6–12]. Their works mainly focused on the development of the DRX evolution model etc, which provided important foundation for predicting the microstructure of the deformed parts.

For the pipe extrusion, ZHANG and YANG [13] studied the change rules of the billet temperature in the extrusion process of the large-scale seamless 6061 aluminum alloy tube by DEFORM-3D and realized the isothermal control of the process. LI et al [14] and DUAN et al [15] simulated the needle piercing extrusion of magnesium alloy and discussed the effects of deformation temperature, extrusion speed and friction on the effective strain, effective stress and extrusion load.

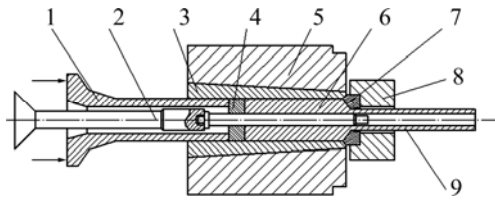


Fig. 1 Schematic diagram of needle piecing extrusion process: 1—Stem; 2—Needle; 3—Liner; 4—Dummy block; 5—Container; 6—Billet; 7—Extrusion die; 8—Die holder; 9—Pipe

LU [16] studied the extrusion process of seamless AISI304 stainless steel pipe by numerical simulation under the platform of DEFORM-2D and experiment, revealed the change rules of temperature field of the bottom die and the extrusion load versus stroke curve, and analyzed the deformation of the material in the extrusion. However, these works mainly focused on the macro deformation rules of the pipe extrusion process. The research on the microstructure evolution, such as dynamic recrystallization behavior, during the extrusion of AISI304 seamless stainless steel pipe has been scant up till now.

So in this study, taking the needle piecing extrusion of the AISI304 stainless steel pipe ($d29 \text{ mm} \times 4.5 \text{ mm}$) as research object, we aim to develop a multi-scale FE model for the process, and then numerically reveal the effect rules of the initial billet temperature and extrusion speed on DRX behavior, thus provide important guidance for the optimal design and steady control of the process in terms of the microstructure of the extruded tube.

2 Multi-scale FE model of needle piecing extrusion process

2.1 Geometry and assembly model

In consideration of the geometry symmetry of the needle piecing extrusion, a 2D axisymmetric multi-scale FE model for the process has been developed. As shown in Fig. 2, the ram is used to model the geometries of the dummy block and the needle, and the die is used to model the geometries of the container and bottom dies. For the extrusion of AISI304 stainless steel pipe with size of $d29 \text{ mm} \times 4.5 \text{ mm}$, a billet ($d50 \text{ mm} \times d20 \text{ mm}/50 \text{ mm}$) is designed. So the diameter of the needle is set as 20 mm; the diameter and height of the dummy block are designed as 50 mm and 20 mm, respectively; and the taper angle is selected as 60° , the calibrating strap length 2.5 mm is used according to Ref. [16].

2.2 Multi-scale model for AISI304 stainless steel

The multi-scale model for AISI304 stainless steel includes the macro constitutive model (Eq. (1)),

describing the high-temperature plastic deformation behavior of the material, and the micro DRX model (Eqs. (2)–(6)), describing the microstructure (such as the DRX volume fraction and grain size) evolution of the material [7].

$$\dot{\varepsilon} = 8.245 \times 10^6 \sigma_p^{6.2583} \exp[-464/(RT)] \quad (1)$$

$$\varepsilon_p = 0.00022 d_0^{0.11} \dot{\varepsilon}^{0.174} \exp[80800/(RT)] \quad (2)$$

$$\varepsilon_c = 0.8 \varepsilon_p \quad (3)$$

$$X_{\text{drx}} = 1 - \exp \left[-0.66 \left(\frac{\varepsilon - \varepsilon_c}{\varepsilon_{0.5}} \right)^{1.46} \right] \quad (4)$$

$$\varepsilon_{0.5} = 3.5 \times 10^{-4} d_0^{0.14} \exp[79400/(RT)] \quad (5)$$

$$d_{\text{drx}} = 3.88 \times 10^3 \{ \dot{\varepsilon} \exp[-118000/(RT)] \}^{-0.254} \quad (6)$$

where $\dot{\varepsilon}$ is strain rate; σ_p is the peak stress; R is the gas constant; T is the deformation temperature (K); ε_p is the peak strain; d_0 is the initial grain size ($d_0=150 \text{ }\mu\text{m}$); ε_c is the critical strain; X_{drx} is volume fraction of DRX; $\varepsilon_{0.5}$ is the strain when 50% of material experiences DRX; d_{drx} is the DRX grain size (μm).

2.3 Calculation conditions and meshes design

The preheating temperature of the ram and die is set as $500 \text{ }^\circ\text{C}$. The convection coefficient between the billet and the surroundings is set as $0.02 \text{ N}/(\text{s}\cdot\text{mm}\cdot^\circ\text{C})$, the heat transfer coefficient is set as $11 \text{ N}/(\text{s}\cdot\text{mm}\cdot^\circ\text{C})$ and the surrounding temperature is $20 \text{ }^\circ\text{C}$ [7]. The shear friction model is used for the extrusion simulation. Glass protective lubricant is always used in the extrusion process and the friction factor can be chosen in the range of $0.047\text{--}0.066$, and the value of 0.05 is always in actual use [17]. In order to reveal the effects of the initial billet temperature T and extrusion speed v on the DRX behavior of the AISI304 stainless steel, the simulation conditions are shown in Table 1.

Table 1 Simulation conditions

Number	Initial billet temperature/ $^\circ\text{C}$	Extrusion speed/ $(\text{mm}\cdot\text{s}^{-1})$
1	1080	200
2	1120	200
3	1160	200
4	1200	200
5	1240	200
6	1160	120
7	1160	160
8	1160	200
9	1160	240
10	1160	280

For the meshes design, the billet, die and ram are meshed by quadrilateral finite elements. To improve the simulation accuracy and efficiency, the mesh refinement is necessary in the main working region, as shown in Fig. 2(b), and the adaptive re-meshing technology is used to ensure the mesh quality.

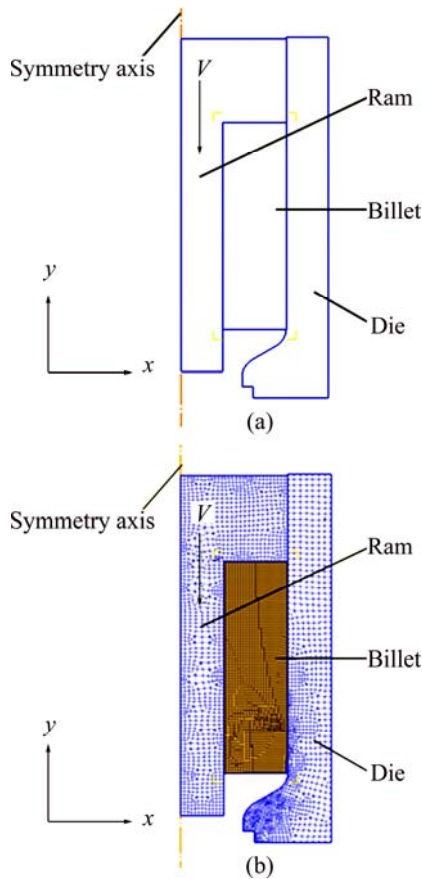


Fig. 2 Multi-scale FE model in DEFORM-2D of needle piecing extrusion: (a) Geometry and assembly model; (b) Initial meshes

2.4 Evaluation of multi-scale FE model

ZHAO [7] experimentally and numerically investigated the DRX behavior of the AISI304 stainless steel and load-stroke curve during forging processes

under different deformation temperatures. The obtained results showed that the relative error of the extrusion loads between experiment and simulation under DEFORM-3D was less than 10%, and a good agreement of the DRX volume fraction between experiment and simulation was observed. This demonstrates that the developed multi-scale FE model in this work has enough accuracy and efficiency for the prediction of the DRX behavior during the extrusion process of seamless AISI304 stainless steel pipe.

3 Results and discussion

3.1 Effect rules of initial billet temperature on DRX

3.1.1 Dynamic recrystallization volume fraction

From the distribution contours shown in Fig. 3, we can observe that the X_{drx} in the middle of the extruded pipe is higher than that on the surface and no dynamic recrystallization occurs for the billet in the container. The reason is that both the temperature and deformation degree in middle of the extruded pipe are higher than those on the surface, as shown in Fig. 4. And we also can see that the X_{drx} on the extruded pipe gradually increases with the rising of the initial billet temperature.

From the distribution curves (Fig. 5) of the X_{drx} in the radial direction of the pipe for the selected sections (Fig. 6) under the temperatures of 1080 °C and 1240 °C, we can see that the X_{drx} rises obviously with the increase of the initial billet temperature; and we also can find that the X_{drx} first increases then decreases in an increasing slope from sections $A-A'$ to $D-D'$ along the radial direction of the extruded pipe. This is because the temperature and effective strain have the change rules as shown in Fig. 7 for the sections $A-A'$ to $D-D'$.

A parameter X_i , defined as the ratio of the material volume V_i whose X_{drx} is over $i\%$ in the extruded pipe to the total volume V_t of the extruded pipe, can be expressed by

$$X_i = V_i / V_t \times 100\% \quad (0 \leq i \leq 100) \tag{7}$$

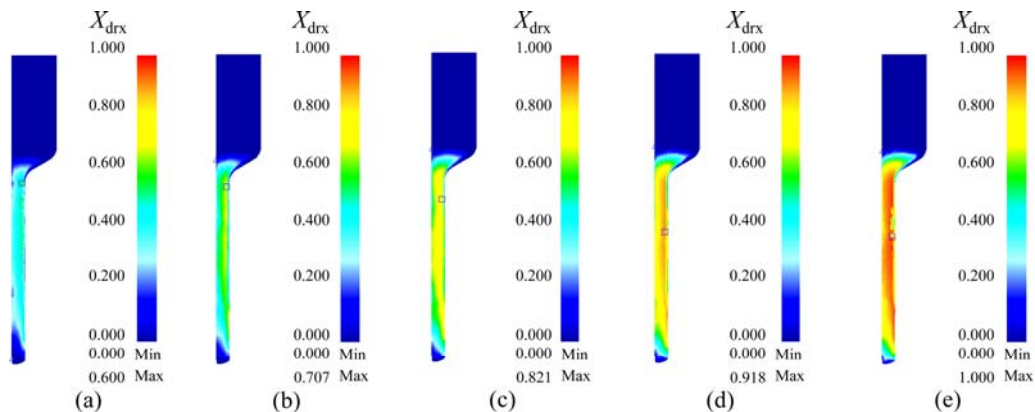


Fig. 3 Distribution contours of X_{drx} under various initial billet temperatures: (a) 1080 °C; (b) 1120 °C; (c) 1160 °C; (d) 1200 °C; (e) 1240 °C

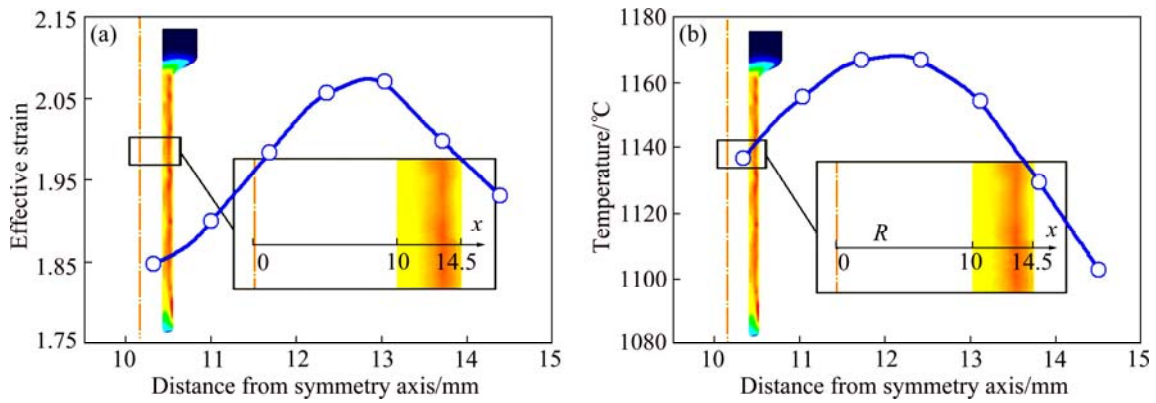


Fig. 4 Distributions of effective strain and temperature in radial thickness direction of extruded pipe: (a) Effective strain; (b) Temperature

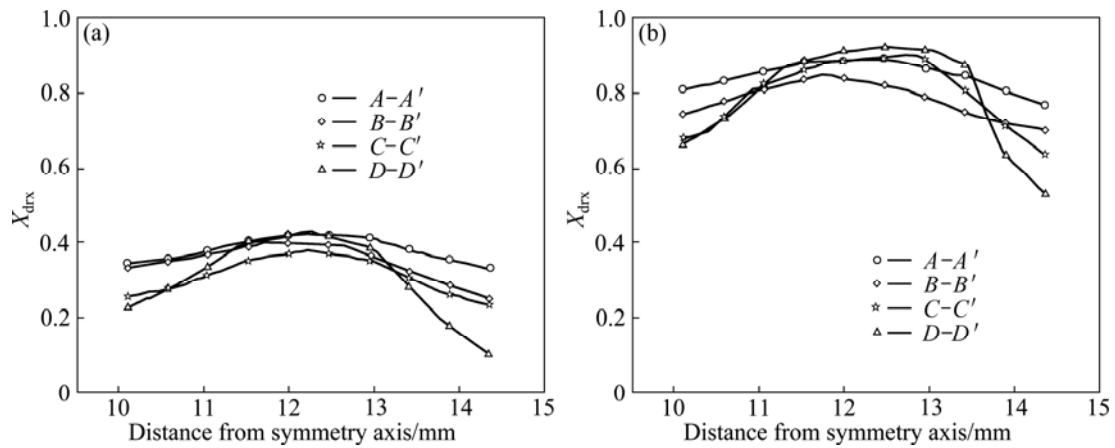


Fig. 5 Distribution curves of $X_{d_{rx}}$ in radial direction of pipe for sections $A-A'$ to $D-D'$ under different temperatures: (a) 1080 °C; (b) 1240 °C

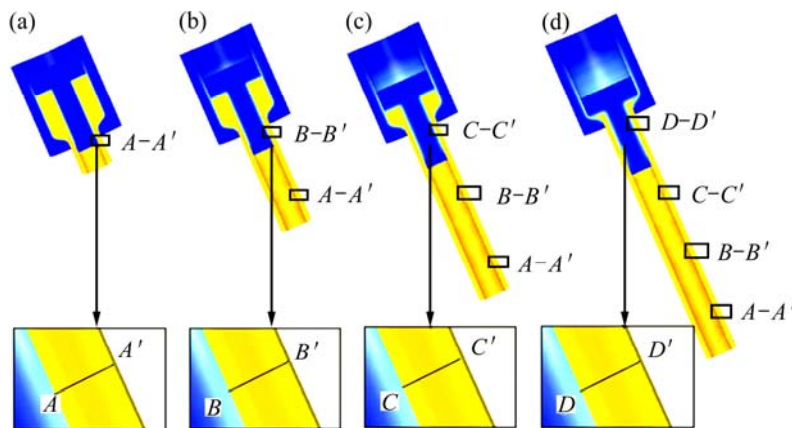


Fig. 6 Schematic diagrams of selected sections $A-A'$ (a), $B-B'$ (b), $C-C'$ (c) and $D-D'$ (d) during needle piercing extrusion process

Figure 8 shows the variation curves of X_{20} , X_{40} , X_{60} and X_{80} versus the initial billet temperature when the extrusion speed is 200 mm/s. We can see that the parameter X_i gradually increases with the increase of the initial billet temperature. This indicates that the material volume whose $X_{d_{rx}}$ is over a certain value in the extruded pipe gradually increases with the increase of the initial

billet temperature. It can also be seen from Fig. 8 that the X_{80} reaches more than 50% when the temperature is 1240 °C but is almost zero when the temperature is lower than 1160 °C.

3.1.2 Average grain size

Figure 9 shows the distribution of the average grain size $d_{average}$ at different initial billet temperatures when

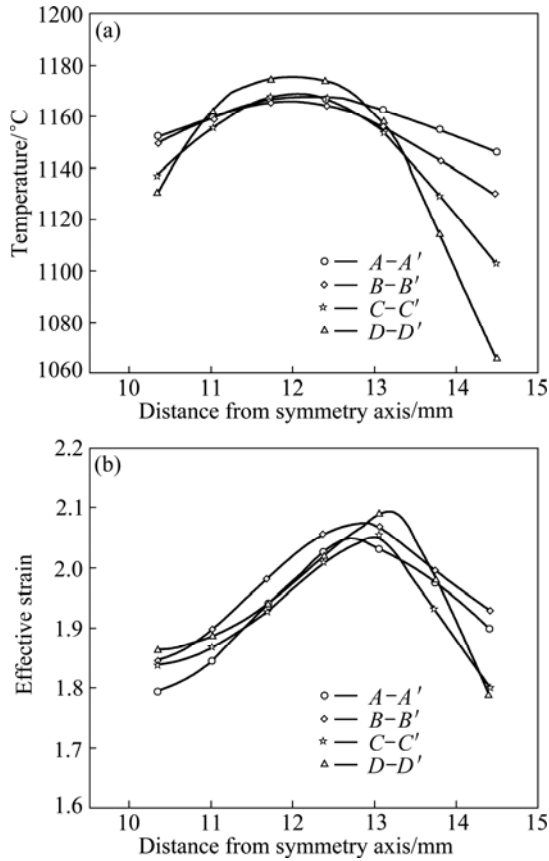


Fig. 7 Distribution curves of temperature and effective strain in radial direction on sections A-A' to D-D': (a) Temperature; (b) Effective strain

the ram stroke is 20 mm. It is seen that the grains of the extruded pipe are refined for different initial billet temperatures due to the dynamic recrystallization. The higher the initial billet temperature, the smaller the average grain size $d_{average}$. And the minimum of $d_{average}$ gradually decreases with the rising of the initial billet temperature while the grain size of the billet in the container remains steady because of no dynamic recrystallization in the material.

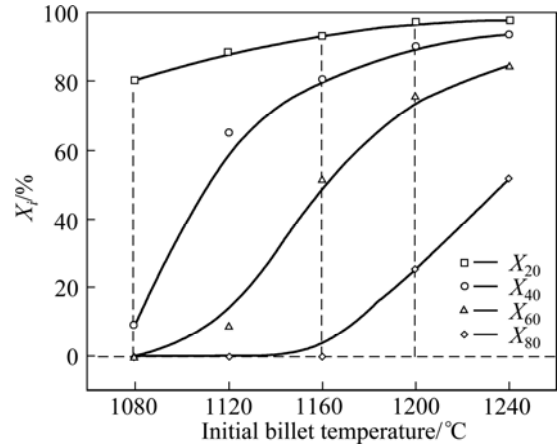


Fig. 8 Curves of X_{20} , X_{40} , X_{60} and X_{80} versus initial billet temperature

From the distribution curves (Fig. 10) of the average grain size $d_{average}$ in the radial direction of the pipe for the selected sections (Fig. 6) under the temperatures of 1080 °C and 1240 °C, we can see that the average grain size obviously decreases with the increase of the initial billet temperature, and first decreases then increases in an increasing slope from sections A-A' to D-D' along the radial direction of the extruded pipe.

The standard deviation (E_{SD}) of the grain size, which reflects nonuniformity of the grain size, is defined by

$$E_{SD} = \sqrt{\sum_{i=1}^N (\chi_i - \chi_a)^2 / (N-1)} \quad (8)$$

where $\chi_a = \sum_{i=1}^N \chi_i / N$, χ_i is the grain size on the i -th node, N is the number of nodes in the extruded pipe at the end of an extrusion process, and χ_a is the average grain size for all the nodes. The larger the value of E_{SD} , the worse the uniformity of the grain size.

Figure 11 shows the variation curve of the E_{SD} with

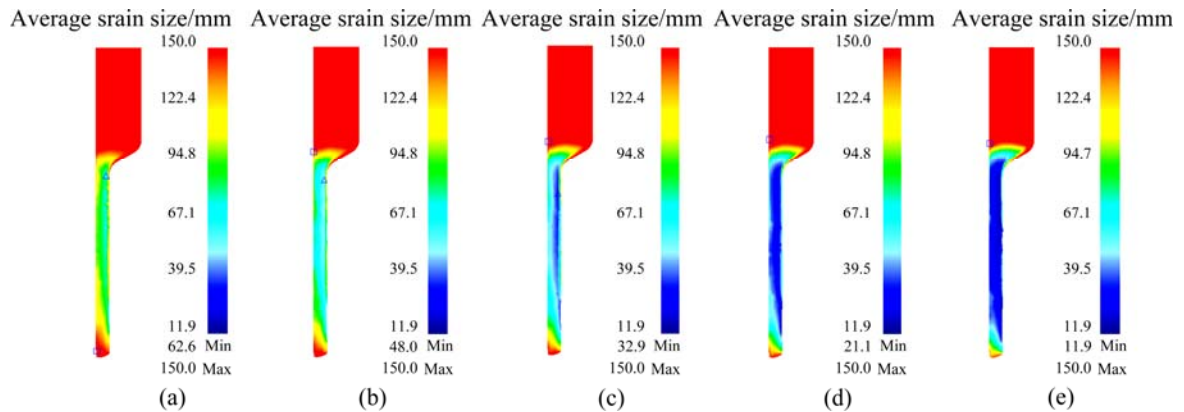


Fig. 9 Distribution contours of $d_{average}$ at different initial billet temperatures: (a) 1080 °C; (b) 1120 °C; (c) 1160 °C; (d) 1200 °C; (e) 1240 °C

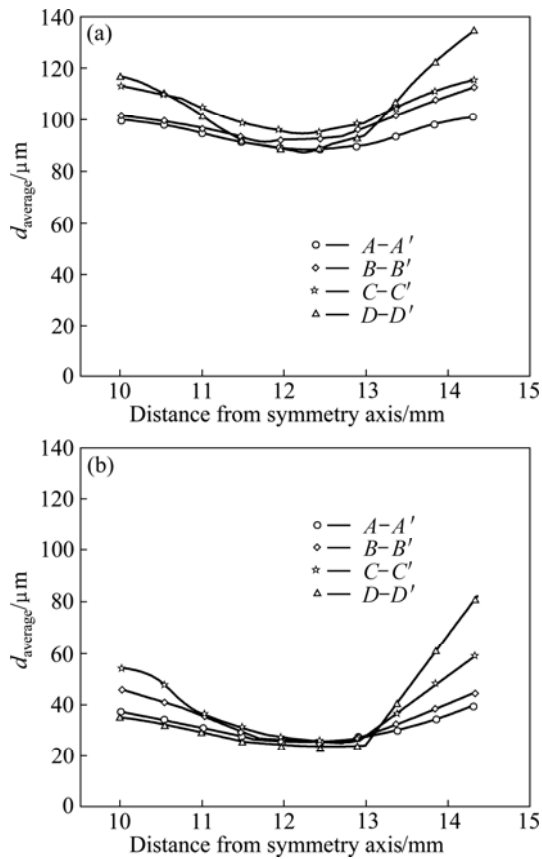


Fig. 10 Distribution curves of $d_{average}$ in radial direction of pipe for sections A-A' to D-D' under temperatures of 1080 °C (a) and 1240 °C (b)

the initial billet temperature. It can be seen that the value of E_{SD} first rises rapidly and then drops a little when the initial billet temperature is over 1160 °C. This means that the uniformity of the grain size firstly becomes worse with the increase of temperature and then reaches the peak when temperature is about 1160 °C. The results provide a significant guideline for the heating schedule design of the extrusion billet in terms of the grain size uniformity.

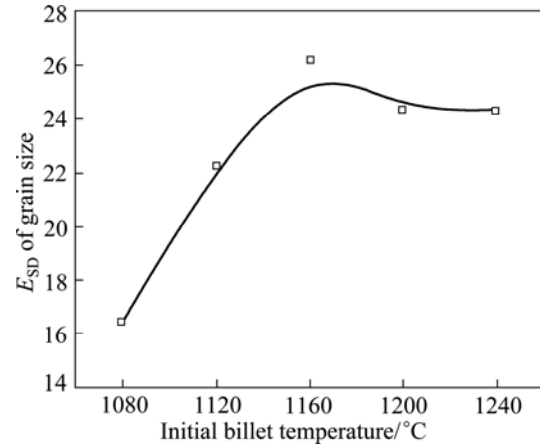


Fig. 11 Variation curve of E_{SD} of grain size versus initial billet temperature

3.2 Effect rules of extrusion speed on DRX

3.2.1 Dynamic recrystallization volume fraction

Figure 12 shows the distributions of the X_{drx} at different extrusion speeds when the ram stroke is 20 mm. It is seen that the maximum of the X_{drx} drops slightly and the region with high X_{drx} becomes smaller and smaller with the increase of the extrusion speed.

From the distribution curves (Fig. 13) of the X_{drx} on the selected sections (Fig. 6), we can see that the X_{drx} drops a little with the rising of the extrusion speed, and first increases then decreases in an increasing slope from sections A-A' to D-D' along the radial direction of the extruded pipe.

Figure 14 shows the variation curves of X_{20} , X_{40} , X_{60} and X_{80} versus the extrusion speed when the initial billet temperature is 1160 °C. We can see that the parameter X_i almost remains unchanged with the increase of the extrusion speed. And the X_{80} almost equals to zero for different extrusion speeds when the initial billet temperature is 1160 °C.

3.2.2 Average grain size

Figure 15 shows the distributions of the average

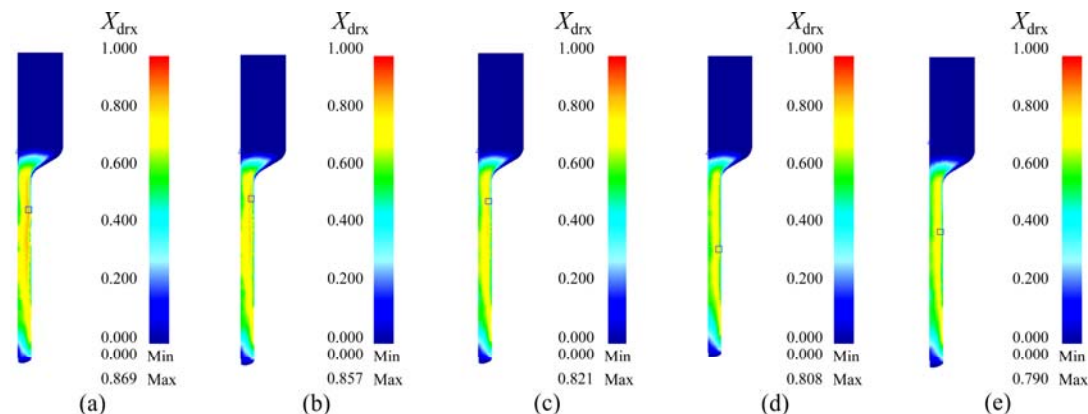


Fig. 12 Distribution contours of X_{drx} at different extrusion speeds: (a) $v=120$ mm/s; (b) $v=160$ mm/s; (c) $v=200$ mm/s; (d) $v=240$ mm/s; (e) $v=280$ mm/s

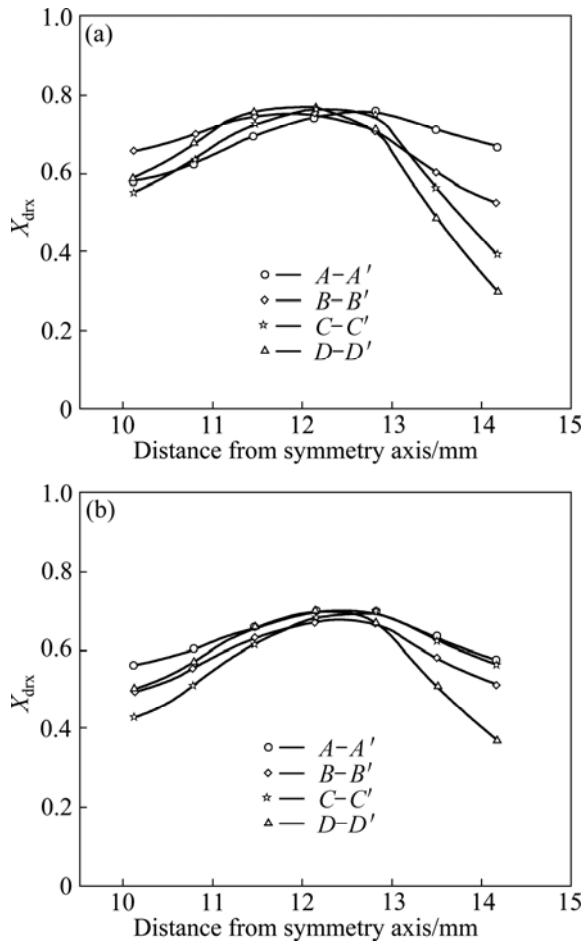


Fig. 13 Distribution curves of X_{dr} in radial direction on sections $A-A'$ to $D-D'$ at $v=120$ mm/s (a) and $v=280$ mm/s (b)

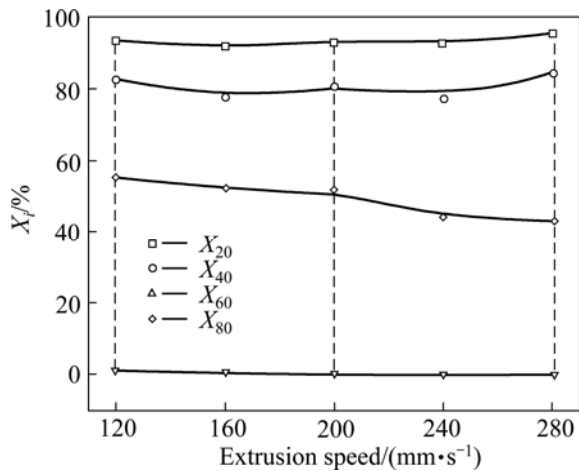


Fig. 14 Curves of X_{20} , X_{40} , X_{60} and X_{80} versus extrusion speed at initial billet temperature of 1160 °C

gain size d_{average} at different extrusion speeds when the ram stroke is 20 mm. It is seen that the minimum of the d_{average} slightly increases with the rising of the extrusion speed and the region with smaller d_{average} becomes smaller.

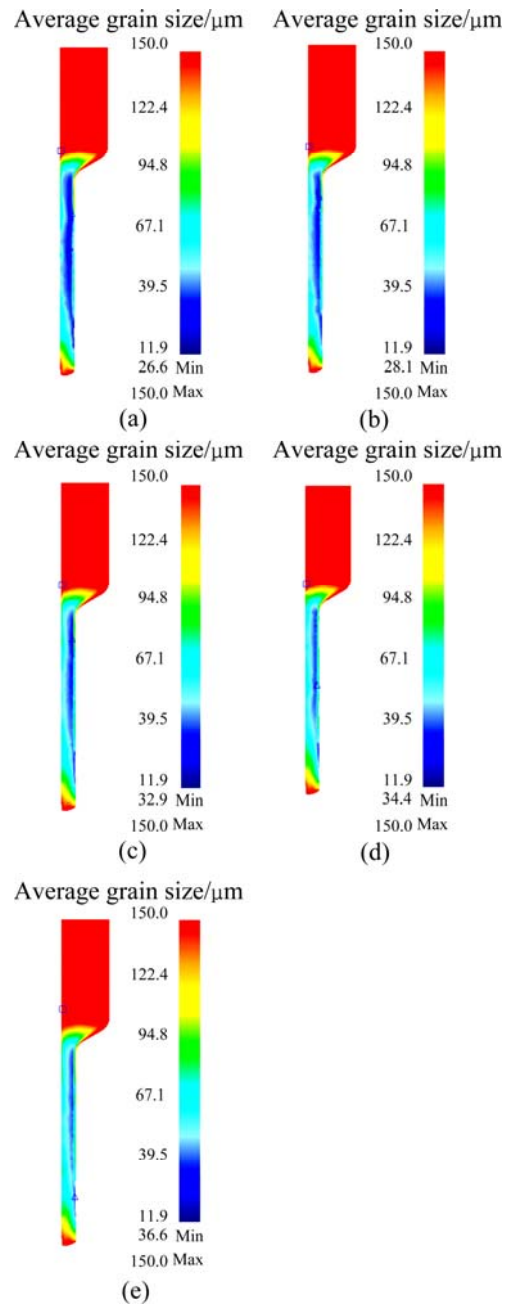


Fig. 15 Distribution contours of d_{average} at different extrusion speeds: (a) $v=120$ mm/s; (b) $v=160$ mm/s; (c) $v=200$ mm/s; (d) $v=240$ mm/s; (e) $v=280$ mm/s

From the distribution curves (Fig. 16) of the d_{average} in the radial direction on the selected sections (Fig. 6), we can find that the d_{average} has negligible changes with the rising of the extrusion speed, and first decreases then increases in an increasing slope from sections $A-A'$ to $D-D'$ along the radial direction of the extruded pipe.

Figure 17 shows the variation curve of the E_{SD} versus the extrusion speed. It is seen that the grain size becomes more homogeneous with the increase of the extrusion speed.

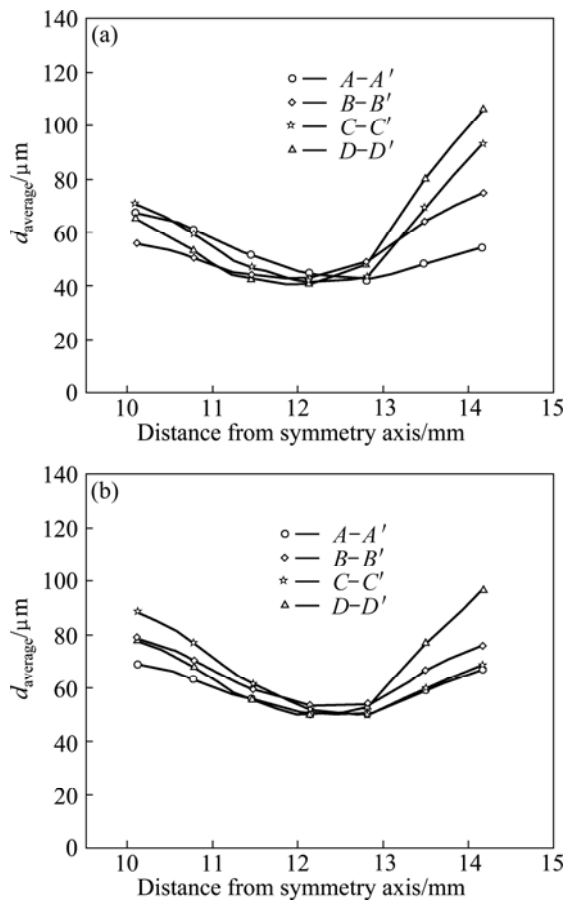


Fig. 16 Distribution curves of d_{averag} in radial direction on sections A-A' to D-D' at $v=120$ mm/s (a) and $v=280$ mm/s (b)

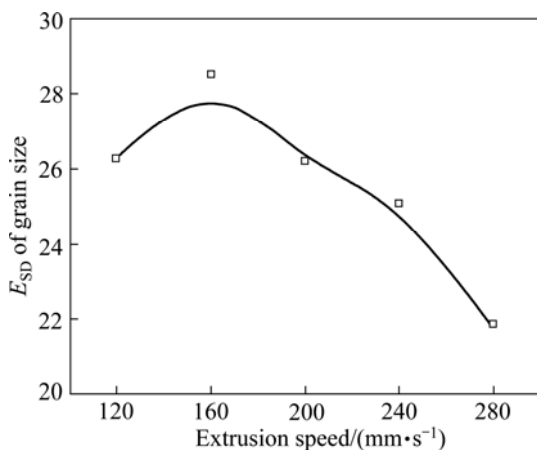


Fig. 17 Variation curve of E_{SD} versus extrusion speed

4 Conclusions

1) The X_{drx} obviously increases with the increase of T , while drops slightly with the increase of v . But the region with high X_{drx} becomes smaller and smaller with the increase of v .

2) The fine grain zone locates in the middle of the extruded pipe. The d_{average} obviously decreases with the increase of T , while has negligible changes with the

variation of v . But the region with smaller d_{average} becomes smaller with the increase of v . The uniformity of the d_{average} becomes worse with the increase of T and the decrease of v .

3) The material volume whose X_{drx} is over a certain value in the extruded pipe gradually increases with the increase of T but has negligible changes with the variation of v .

References

- [1] XIAO Ji-mei. Metallography problem of stainless steel [M]. Beijing: Metallurgical Industry Press, 2006. (in Chinese)
- [2] Chinese Mechanical Engineering Society Forging Association. Forging manual [M]. Beijing: China Machine Press, 2002. (in Chinese)
- [3] SHI Feng, WANG Li-jun, CUI Wen-feng. Aging precipitation and recrystallization in high-nitrogen austenitic stainless steel [J]. Transactions of Nonferrous Metals Society of China, 2009, 19: s569–s572.
- [4] YAN Sheng-xiang, ZHONG Qian-xia. Development of manufacturing technology for stainless steel tubes [J]. Steel Pipe, 2008, 37(2): 5–10. (in Chinese)
- [5] ZHONG Qian-xia, YAN Sheng-xiang. Domestic demand for stainless steel tubes and development trend of manufacturing technologies for stainless steel tubes both at home and abroad [J]. Steel Pipe, 2002, 31(5): 1–8. (in Chinese)
- [6] DEGHAN-MANSHADI A, BARNETT M R, HODGSON P D. Recrystallization in AISI304 austenitic stainless steel during and after hot deformation [J]. Materials Science and Engineering A, 2008, 485(1–2): 664–672.
- [7] ZHAO Xiao-dong. Dynamic recrystallization research of AISI304 austenitic during hot deformation [D]. Taiyuan: Taiyuan University of Science and Technology, 2009. (in Chinese)
- [8] GE Dong-sheng, LIU Jie, FAN Guang-wei, ZHAO Xiao-dong, YAO Xiao-fei. Dynamic crystal structure characteristics of AISI304 austenitic stainless steel cast in heat distortion [J]. Research Studies on Foundry Equipment, 2008(5): 15–20. (in Chinese)
- [9] XIONG Jia-qiang, XIE Gang, TANG Guang-bo. Research on dynamic recrystallization of austenite and flow stress during hot deformation process of AISI304 stainless steel [J]. Yunnan Metallurgy, 2008, 37(5): 37–42. (in Chinese)
- [10] XU S G, CAO Q X. Numerical simulation of the microstructure in the ring rolling of hot steel [J]. Journal of Materials Processing Technology, 1994, 43(2–4): 221–235.
- [11] KIM S I, YOO Y C. Dynamic recrystallization behavior of AISI AISI304 stainless steel [J]. Materials Science and Engineering A, 2001, 311(1–2): 108–113.
- [12] BELYAKOV A, MIURA H, SAKAI T. Dynamic recrystallization under warm deformation of a AISI304 type austenitic stainless steel [J]. Materials Science and Engineering A, 1998, 255(1–2): 139–140.
- [13] ZHANG Jun, YANG He. Research on the influence of deformation speed on 6061 aluminium alloy large-size seamless tube extrusion by means of 3D FEM simulation [J]. Heavy Machinery, 2004(5): 40–45. (in Chinese)
- [14] LI Lin-lin, ZHANG Zhi-min, XUE Yong. Study on numerical simulation of extrusion forming of Mg alloy AZ31 tubing [J]. China Metalforming Equipment & Manufacturing Technology, 2006, 41(2): 70–72. (in Chinese)

- [15] DUAN Ya-li, ZHANG Zhi-min, XUE Yong. Analysis of isothermal extrusion technology and die design of AZ31 magnesium alloy thin-walled tubes [J]. China Metalforming Equipment & Manufacturing Technology, 2007, 42(2): 55–53. (in Chinese)
- [16] LU Ri-yang. Die structure and process parameters optimization of hot extrusion for austenitic stainless steel pipes based on numerical simulation [D]. Nanjing: Jiangsu University, 2009. (in Chinese)
- [17] LIU Zhang-yong, ZHANG Ren-ji, YAN Yong-nian. Glass lubrication technology in steel hot extrusion [J]. Hot Working Technology, 2010, 39(5): 108–11. (in Chinese)

AISI304 不锈钢管穿孔针挤压动态再结晶规律

郭良刚¹, 董可可¹, 张保军¹, 杨合¹, 郑文达², 刘雄伟³

1. 西北工业大学, 凝固技术国家重点实验室, 西安 710072;

2. 中国重型机械研究院有限公司, 西安 710032;

3. Sustainable Engineering, University of Cumbria, Enercus Campus, Workington, CA14 4JW, UK

摘要: 在 AISI304 不锈钢管穿孔针挤压成形过程中, 揭示挤压坯料的动态再结晶规律, 是实现动态再结晶行为的有效控制, 从而获得具有细晶及合格微观组织的管材的基础和关键。基于 DEFORM-2D 软件平台, 以 $d29\text{ mm} \times 4.5\text{ mm}$ AISI304 不锈钢管的穿孔针挤压过程为研究对象, 首先建立了该过程适用、可靠的多尺度有限元分析模型; 通过大量的数值模拟分析, 阐明了关键挤压成形参数(即坯料初始温度和挤压速度)对挤压坯料的动态再结晶体积分数、平均晶粒尺寸及其分布的影响规律, 所得结论为根据挤压管材的微观组织对 AISI304 不锈钢管穿孔针挤压成形过程进行优化设计与稳健控制提供了重要理论依据和指南。

关键词: AISI304 不锈钢; 动态再结晶; 穿孔针挤压; 建模与仿真; 微观组织; 晶粒细化

(Edited by HE Yun-bin)